Thermodynamic and Structural Characterization of the Transformation from a Metastable Low-Density to a Very High-Density Form of Supercooled TIP4P-Ew Model Water

Dietmar Paschek,* Andreas Rüppert, and Alfons Geiger[a]

We explore the phase diagram of the metastable TIP4P-Ew liquid model water from 360 K down to 150 K at densities ranging from 0.950 to 1.355 g cm^{-3}. In addition to the low-density/high-density (LDL/HDL) liquid–liquid transition, we observe a structural high-density/very high-density (HDL/VHDL) transformation for the lowest temperatures at 1.30 g cm^{-3}. The characteristics of the isobars and isotherms suggest the presence of a stepwise HDL/VHDL transition with first-order-like appearance. In addition, we also identify an apparent pretransition at 1.24 g cm^{-3}, which suggests that the experimentally detected LDA/VHDA transformation might evolve into a multiple-step process with different local structures representing local minima in the free-energy landscape. Such a scenario is supported by a pronounced correlation between the isothermal density dependence of the pressure, with a stepwise increase of the oxygen coordination number, due to the appearance of interstitial water molecules.

1. Introduction

Experimental and theoretical studies conducted over the past 16 years have led to the interpretation that the anomalies of water stem from the existence of two metastable liquid forms of water buried in the deeply supercooled region (see reviews by Stanley and Debenedetti[1,2]). The two different liquids have their counterparts in the glassy state, that is, the high-density (HDA) and low-density amorphous (LDA) forms of ice.[3,4] However, it is still an open question how exactly the different forms of amorphous ice and supercooled liquid water are connected, since the "no-man's land" largely prohibits direct experimental access.[2] Therefore, starting with the work of Poole et al. in 1992, computer simulation studies have proposed a picture of a first-order liquid–liquid phase transition between two metastable liquids ending up at a metastable critical point.[5,6] Although singularity-free scenarios may also explain the properties of supercooled water,[2] there is experimental support for the liquid–liquid critical-point hypothesis from the changing slope of the metastable melting curves observed for different ice polymorphs.[7,8]

Meanwhile, a very high-density form (VHDA) of amorphous ice was observed and shown to be distinct from HDA.[9] Neutron-scattering data revealed that the transformation from HDA to VHDA is accompanied by an increasing population of interstitial water molecules in an O···O distance interval between 3.1 and 3.3 Å.[10] Simulation studies suggest that VHDA ice should be considered as the amorphous solid counterpart to the high-density liquid water phase under ambient conditions, rather than HDA.[11,12] Koza et al.[13] demonstrated, by using inelastic neutron scattering, that HDA and VHDA ice appear to be heterogeneous on the length scale of nanometers, and that different forms of HDA ice are obtained, depending on the exact preparation process.[13] By annealing HDA ice at normal pressure Tulk et al.[14] observed a multitude of (meta-stable) amorphous ice states. Finally, recent experimental stud-

ies by Loerting et al. suggest the presence of an apparent higher order phase transition between HDA and VHDA ice.[15,16] Extensive Gibbs-ensemble Monte Carlo computer simulations of Brovchenko et al.[17–19] suggest the coexistence of up to four different phases of water. Their results, however, also show that the obtained phase diagrams depend critically on details of the water model, and in particular on the treatment of cutoff corrections for long-range forces.[18]

Here we present extensive thermophysical data on the deeply supercooled liquid state of the TIP4P-Ew water model.[20] TIP4P-Ew seems to be an ideal candidate, since it not only reproduces well the thermodynamic and structural properties of the liquid phase[20] (including a boiling point at 370 K[21]), but the TIP4P family of models also describe remarkably well the different ice polymorphs[22–24] and qualitatively reproduces the entire phase diagram of crystal solid water up to about 1 GPa. Hence there is hope that TIP4P-Ew keeps the right balance between local order and volume also for the amorphous states. Recently, attempts to study the HDA to VHDA transition by computer simulations suggested a continuous structural transformation.[25] To enhance the sampling at low temperatures, we present parallel tempering simulations of an extended ensemble of states,[26] applying the technique of volume–temperature replica exchange molecular dynamics simulation (VTREMD), which we recently used to study the properties of the metastable forms of the supercooled liquid of TIP5P-E model[27] water.[28]

[a] Dr. D. Paschek, A. Rüppert, Prof. Dr. A. Geiger
Physikalische Chemie, Fakultät Chemie, TU Dortmund
Otto-Hahn-Str. 6, D-44227 Dortmund (Germany)
Fax: (+49) 231-755-3748
E-mail: dietmar.paschek@uni-dortmund.de

2. Replica Exchange Molecular Dynamics Simulations

Replica exchange molecular dynamics (REMD) is an enhanced sampling technique based on the parallel tempering Monte Carlo method,[2–31] wherein multiple copies (or replicas) of identical systems are simulated in parallel at different temperatures. The REMD scheme[32] is a MD simulation technique that enhances sampling by about two orders of magnitude.[33] State-swapping moves between two states *i* and *j* are accepted with a probability given by Equation (1):

$$P_{acc} = \min\left\{ 1, \exp\left[\begin{array}{l} \beta_i\left(U(\vec{s}_i^N; L_i) - U(\vec{s}_j^N; L_i)\right) \\ +\beta_j\left(U(\vec{s}_j^N; L_j) - U(\vec{s}_i^N; L_j)\right) \end{array} \right] \right\} \quad (1)$$

where $\vec{s}_i^N$ represents the set of scaled coordinates $\vec{s}_N = L^{-1}\vec{r}_N$ of the entire *N*-particle system belonging to state *i*, $U(\vec{s}_i^N; L_i)$ is the potential energy of configuration $\vec{s}_i^N$ at volume $V_i = L_i^3$, and $U(\vec{s}_i^N; L_j)$ is the configurational energy belonging to $\vec{s}_i^N$, scaled to volume V_j. Whether a state-swapping move or an MD move is executed is chosen at random with a probability of 0.2 for selecting state-swapping moves (approximately every fifth time step, two neighboring states are picked on average). For our simulation we consider a grid of 28×23 (*V*,*T*) states[34] (644 states in total). Each replica represents a MD simulation of 256 molecules in the *NVT* ensemble. A 2 fs time step was used and a Nosé–Hoover[35,36] thermostat was employed with a time coupling of $\tau_T = 0.5$ ps. TIP4P-Ew bond constraints were solved by using the SETTLE procedure.[37] The electrostatic interactions are treated by Ewald summation[38] with a cutoff of 0.9 nm and a 18×18×18 mesh with fourth-order interpolation. Lennard–Jones cutoff corrections for energy and pressure were considered. The simulations were carried out with the GROMACS 3.2 simulation program (www.gromacs.org), modified by us to allow (*V*,*T*)-state swapping. The temperature tiling was chosen to maintain an acceptance ratio of about 0.2 for state swapping.

Starting from a set of equilibrated initial configurations obtained under ambient conditions, the simulation was conducted for 50 ns to provide a total of 32.2 μs of trajectory data. The average time interval for each state between two state-exchange attempts was about 3 ps. The overall shape of the phase diagram presented here is already well established after only 2 ns of simulation time. However, since the configurational sampling of the lower-*T* states happens almost exclusively by exchange with replicas coming from higher temperatures, the resolution of fine details of the *PVT* diagram requires a long simulation run. The simulation took about 100 days on 20 processors of our Intel Xeon 3.05 GHz Linux cluster. All data reported here were averaged over the final 45 ns of the simulation.

3. Discussion

Figure 1 shows the phase diagram of liquid TIP4P-Ew water as a contour plot of the $P(\rho,T)$ data. The TIP4P-Ew phase diagram exhibits a first-order low-density/high-density liquid–liquid
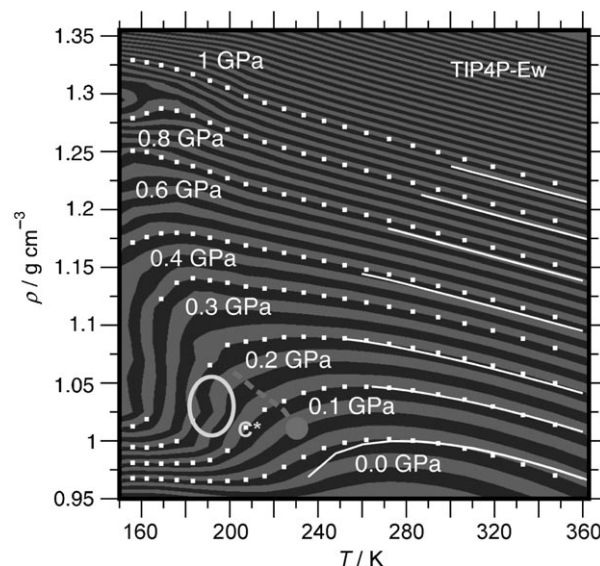

Figure 1. $P(\rho,T)$ surface of liquid TIP4P-Ew water.[39] The spacing between different contour colors corresponds to a pressure drop of 25 MPa. Selected isobars are indicated by dotted lines. The solid lines give the experimental isobars for 0.1 MPa, and 0.1, 0.2, 0.4, 0.6, 0.8, and 1.0 GPa.[40] The ellipse indicates the LDL/HDL critical region for TIP4P-Ew with $C^* \approx$ (0.175 GPa, 190 K, 1.03 g cm^{-3}). The large filled circle and the heavy dashed line indicate the metastable critical point and HDL/LDL transition line for D$_2$O according to Mishima,[8] projected on the TIP4P-EW $P(\rho,T)$ surface.

phase transition ending in a metastable critical point C^*. The ellipse denotes the region in which the LDL/HDL critical point is apparently located. Due to a finer *T* grid at lower temperatures and longer simulation times, we have improved the sampling of the low-*T* states compared to our recent study on the five-site TIP5P-E model.[28] Figure 1 demonstrates that TIP4P-Ew reproduces the experimental phase diagram of liquid water much better than the TIP5P-E model;[28] it almost quantitatively matches the compressibility and thermal expansivity of water up to pressures in the gigapascal range. Figure 1 shows that the van der Waals looplike overshooting of the $P(\rho,T)$ isotherm, as observed in the HDL/LDL coexistence region of the TIP5P-E model,[28] is almost completely flattened out in the present study, that is, convergence is improved. Figure 1 also shows the LDL/HDL transition line and critical point obtained experimentally by Mishima[8] for D$_2$O. Since the densities of the experimental coexistence line are essentially not known, we projected the pressures reported by Mishima onto the TIP4P-Ew $P(\rho,T)$ surface. We find a temperature difference between the two metastable critical points of about 30–40 K, which corresponds roughly to the temperature difference between the ice-I_h melting lines of TIP4P-Ew and D$_2$O.[23]

In addition to the LDL/HDL transition, we denote in Figure 1 the appearance of another (HDL/VHDL) steplike liquid–liquid

transition at 1.30 g cm^{-3} and about 165 K. The apparent metastable transition is identified by a van der Waals loop-type behavior of P versus ρ shown in Figure 2a. Figure 2b presents
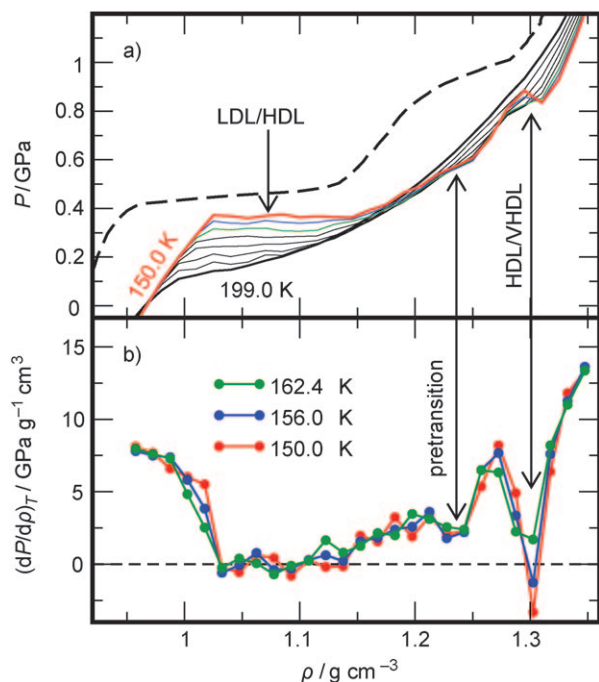
Figure 2. a) Isotherms $P(\rho,T)$ for the eight lowest temperatures. The dashed line represents the compression curve of amorphous ice at 125 K according to Loerting et al.[15] b) $\partial P(\rho,T)/\partial\rho)_T$ for the three lowest temperature isotherms. The arrows indicate the location of the LDA/HDA and HDA/VHDA transitions, as well as the apparent pretransition.

the derivative $(\partial P(\rho,T)/\partial\rho)_T$ of the lower-T isotherms, in which the HDL/VHDL transition is characterized by a pronounced dip. In addition to the fully developed first-order transition at 1.30 g cm^{-3}, a shoulder at about 1.24 g cm^{-3} (Figure 2a) corresponds to a less well pronounced dip in Figure 2b. Both diagrams indicate the emergence of an additional, yet not fully developed, transition around 1.24 g cm^{-3}, which we refer here to as the HDL/VHDL pretransition. Note, however, that the time evolution of the pressure (averaged over time slices of one nanosecond) shown in Figure 3 seems to indicate long-term fluctuations on a timescale of several nanoseconds for the lowest temperatures. This must be attributed to the fact that configurational sampling under these low-temperature conditions happens solely due to the state exchange of replicas diffusing in from higher temperatures. The shown degree of convergence of the REMD simulation ensures that the large features of the phase diagram, such as the LDL/HDL transition, are established reliably. We cannot fully rule out, however, that the more detailed smaller features discussed above might change their character (first-order/second-order) if the simulation were extended.

Our simulations are in qualitative agreement with the experimental compression curve of amorphous water obtained at 125 K (Figure 2a). However, there is a shift of about
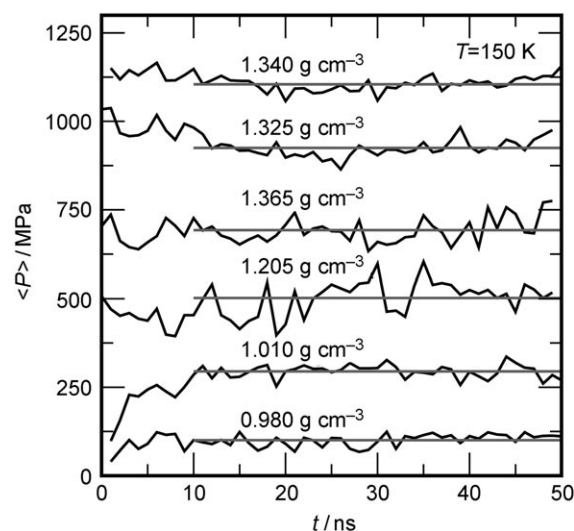
Figure 3. Time evolution of the $P(\rho,T)$ data of liquid TIP4P-Ew water for selected densities at $T = 150$ K. Each data point represents averaging over 1 ns of trajectory data.
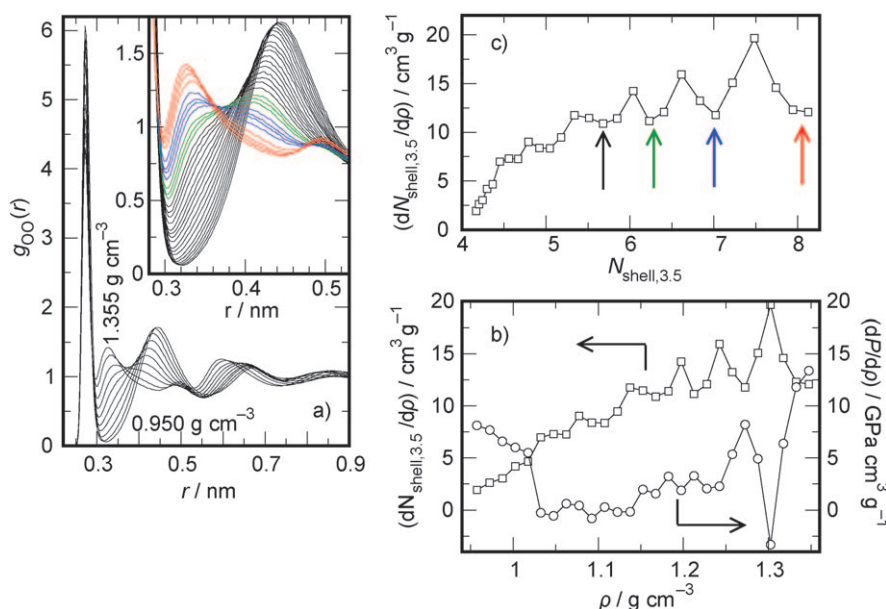
0.06 g cm^{-3} between the experimental and simulated data sets. The elastic compression of 0.10 g cm^{-3} GPa^{-1} for VHDA obtained by Loerting et al.[15] is comparable to that of the 0.08 g cm^{-3} GPa^{-1} (the inverse of the data shown in Figure 2b) of the VDHL phase observed here. The larger elastic compression found for HDA (ca. 0.14 g cm^{-3} GPa^{-1} [15]) is also qualitatively in accordance with our simulation data. Moreover, the slightly asymmetric shape of the HDA/VHDA transition observed by Loerting et al.[15] in the density interval between 1.18 and 1.30 g cm^{-3} does not seem to rule out the presence of a softer transition or pretransition in the density range of 1.22 to 1.24 g cm^{-3} and a sharper transition at about 1.28 g cm^{-3}.

Figures 4 and 5 show how the observed transitions are related to structural changes in the local environment of the water molecules. Figure 4 compares site–site radial distribution functions for densities corresponding to HDL and VHDL with experimental data obtained for HDA and VHDA by Finney and coworkers.[10] The simulated pair distribution functions involving oxygen seem to be significantly too sharp, and this indicates a too strongly repulsive (hard-sphere-like) water–water interaction. However, the features beyond the first minimum change in a quite similar fashion in the TIP4P-Ew liquid as they do in the amorphous ice. Figure 5a depicts the O–O pair correlation functions for water at 150 K as a function of density. The inset in Figure 5a focuses primarily on the changes in the so-called interstitial water region between 0.3 and 0.35 nm, located between the first and second maxima indicative of the tetrahedral network observed at low pressures. In line with structural data obtained from neutron scattering experiments,[10] we observe the appearance of a peak in the interstitial region as pressure increases. Moreover, with increasing density undulations appear in the water coordination number. In the inset in Figure 5a these undulations appear as larger gaps between the individual evenly spaced $g(r)$ curves. For better recognizability these increased gaps are indicated by changes in color.
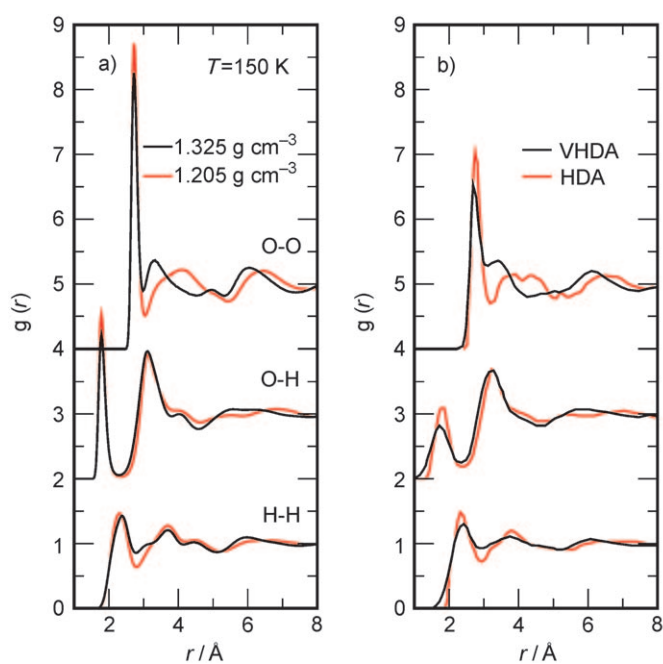
Figure 4. a) Atom–atom radial pair distribution functions for TIP4P-EW obtained at $T = 150$ K for the indicated densities. b) Experimental radial distribution functions obtained for high- and very high-density amorphous ice.[10]

The magnitude of the variation in the local density is shown in Figure 5 b by plotting the derivative of the water O–O coordination number for $r \leq 0.35$ nm with respect to the density $(\partial N_{3.5}/\partial\rho)_T$. Comparing in Figure 5 b the coordination number data with the $(\partial P(\rho,T)/\partial\rho)_T$ line, we find that the observed

HDL/VHDL transitions are exactly accompanied by a stepwise increase of the water coordination number. Moreover, plotting the $(\partial N_{3.5}/\partial\rho)_T$ data as a function of the coordination number $N_{3.5}$ (Figure 5 c) reveals that the HDL/VHDL transition is accompanied by an increase from seven to eight water molecules in the sphere of 0.35 nm around a central water molecule. At the HDL/VHDL pretransition we find only a fractional increase of about 0.75 water molecules on average. Further wiggles in $(\partial N_{3.5}/\partial\rho)_T$ suggest that there is at least one more step in the occupation number at even lower densities.

Figure 6 illustrates the structural changes of the local water environment along the HDL/VHDL pre- and main transitions as observed in our computer simulations. In line with experimental finding, the first coordination shell of water ($r \leq 0.3$ nm) is found to consist of four tetrahedrally arranged water molecules.[10] These positions, which are represented by the yellow regions, are the only ones occupied in the LDL state (not shown here). With increasing pressure, water penetrates the interstitial region ($0.3 \leq r \leq 0.35$ nm), arranged in lobes around the positions occupied by the first-shell water molecules. However, even at the highest densities no more than about four water molecules fill the interstitial positions, that is, the lobe-type positions can only by partially occupied. Figure 6 a indicates that for HDL water the interstitial molecules are located on the "anti-tetrahedral" positions, on the centers of the faces of the tetrahedron formed by the first-shell water molecules. Figure 6 b,d indicate that along the pretransition interstitial water predominantly inserts into these anti-tetrahedral positions, whereas during the HDL/VHDL main transition the lobes are increasingly completed by filling the gaps between two anti-tetrahedral sites. Figure 6 e, which shows four nearest-neighbor water molecules and three water molecules in anti-tetrahedral coordination, exemplifies this scenario. Water molecules occupying connecting lobe positions apparently form hydrogen bonds with each other.

4. Conclusions

Our simulations indicate the presence of a major HDL/LDL transition in supercooled water, which is responsible for the anomalous thermodynamic behavior of water under ambient conditions. However, with decreasing temperature, the $P(\rho,T)$ surface of water becomes increasingly corrugated and develops further steplike transformations, such as the HDL/VHDL pre- and main transitions—and possibly more at even lower temperatures. The onset of these transformations is appa-
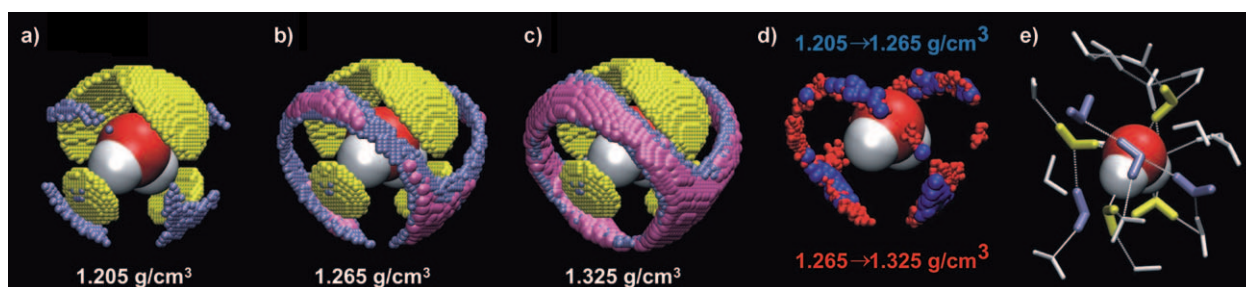

Figure 5. a) O–O radial pair distribution functions $g(r)$ for 150.0 K showing every third density. The inset shows all O–O $g(r)$ for the "interstitial region" for 150.0 K. Changes in color indicate gaps between the $g(r)$ lines. b) Derivative of the pressure with respect to the density for the 150.0 K isotherm and derivative of the water coordination number ($r_{OO} \leq 0.35$ nm) with respect to the density. c) Derivative of the water coordination number ($r_{OO} \leq 0.35$ nm) with respect to the density as a function of the coordination number.

Figure 6. a–c) Three-dimensional distribution of water density around a central water molecule. Each small sphere represents a volume element with a water number density larger than 100 nm^{-3}, whereas the larger (mauve) spheres indicate densities exceeding 130 nm^{-3}. Yellow indicates the first shell ($r \leq 0.3$ nm), and ice blue and mauve indicate interstitial water ($r < 0.3 \leq 0.35$ nm). Densities are indicated, $T = 150$ K. d) Volume elements showing a number density increase of more than 45 nm^{-3} when the density is increased from 1.205 to 1.265 g cm^{-3} (blue) and from 1.265 to 1.325 g cm^{-3} (red) at 150.0 K. e) Snapshot of a randomly selected solvation shell of a water molecule, 1.325 g cm^{-3} at 150.0 K. Color coding is as in (a).

rently tightly related to a distinct increase in the local coordination of the water molecules. Hence, we propose a two-region scenario for supercooled water: A very low-temperature region with several distinct structural transitions, which is typically probed by studies on the amorphous forms of water,[9,13–15] and a "medium"-temperature region, where—due to increased thermal energy—these transitions are covered and two major liquid forms of metastable water (namely, LDL and HDL) are found to be in equilibrium.

Acknowledgements

[1] P. G. Debenedetti, H. E. Stanley, *Phys. Today* **2003**, *56*, 40–46.
[2] P. G. Debenedetti, *J. Phys. Condens. Matter* **2003**, *15*, R1669–R1726.
[3] O. Mishima, L. D. Calvert, E. Whalley, *Nature* **1984**, *310*, 393–395.
[4] T. Loerting, N. Giovambattista, *J. Phys. Condens. Matter* **2006**, *18*, R919–R977.
[5] P. H. Poole, F. Sciortino, U. Essmann, H. E. Stanley, *Nature* **1992**, *360*, 324–328.
[6] H. Tanaka, *Nature* **1996**, *380*, 328–330.
[7] O. Mishima, H. E. Stanley, *Nature* **1998**, *396*, 329–335.
[8] O. Mishima, *Phys. Rev. Lett.* **2000**, *85*, 334–336.
[9] T. Loerting, C. Salzmann, I. Kohl, E. Mayer, A. Hallbrucker, *Phys. Chem. Chem. Phys.* **2001**, *3*, 5355–5357.
[10] J. L. Finney, D. T. Bowron, A. K. Soper, T. Loerting, E. Mayer, A. Hallbrucker, *Phys. Rev. Lett.* **2002**, *89*, 205503.
[11] N. Giovambattista, H. E. Stanley, F. Sciortino, *Phys. Rev. Lett.* **2005**, *94*, 107803.
[12] N. Giovambattista, H. E. Stanley, F. Sciortino, *Phys. Rev. E* **2005**, *72*, 031510.
[13] M. M. Koza, B. Geil, K. Winkel, C. Köhler, F. Czeschka, M. Scheuermann, H. Schober, T. Hansen, *Phys. Rev. Lett.* **2005**, *94*, 125506.
[14] C. A. Tulk, C. J. Benmore, J. Urquidi, D. D. Klug, J. Neuefeind, B. Tomberli, P. A. Egelstaff, *Science* **2002**, *297*, 1320–1323.
[15] T. Loerting, W. Schustereder, K. Winkel, C. Salzmann, I. Kohl, E. Meyer, *Phys. Rev. Lett.* **2006**, *96*, 025701.
[16] K. Winkel, M. S. Elsaesser, E. Mayer, T. Loerting, *J. Chem. Phys.* **2008**, *128*, 044510.
[17] I. Brovchenko, A. Geiger, A. Oleinikova, *J. Chem. Phys.* **2003**, *118*, 9473–9476.
[18] I. Brovchenko, A. Geiger, A. Oleinikova, *J. Chem. Phys.* **2005**, *123*, 044515.
[19] I. Brovchenko, A. Oleinikova, *J. Chem. Phys.* **2006**, *124*, 164505.
[20] H. W. Horn, W. C. Sope, J. W. Pitera, J. D. Madura, T. J. Dick, G. L. Hura, T. Head-Gordon, *J. Chem. Phys.* **2004**, *120*, 9665–9678.
[21] H. W. Horn, W. C. Swope, J. W. Pitera, *J. Chem. Phys.* **2005**, *123*, 194504.
[22] E. Sanz, C. Vega, J. L. F. Abascal, *Phys. Rev. Lett.* **2004**, *92*, 255701.
[23] C. Vega, E. Sanz, J. L. F. Abascal, *J. Chem. Phys.* **2005**, *122*, 114507.
[24] C. Vega, J. L. F. Abascal, E. Sanz, L. G. MacDowell, C. McBride, *J. Phys. Condens. Matter* **2005**, *17*, S3283–S3288.
[25] R. Martoňák, D. Donadio, M. Parrinello, *J. Chem. Phys.* **2005**, *122*, 134501.
[26] E. Marinari, G. Parisi, *Europhys. Lett.* **1992**, *19*, 451–458.
[27] S. W. Rick, *J. Chem. Phys.* **2004**, *120*, 6085–6093.
[28] D. Paschek, *Phys. Rev. Lett.* **2005**, *94*, 217802.
[29] U. H. E. Hansmann, *Chem. Phys. Lett.* **1997**, *281*, 140–150.
[30] U. H. E. Hansmann, Y. Okamoto, *Curr. Opin. Struct. Biol.* **1999**, *9*, 177–183.
[31] D. Frenkel, B. Smit, *Understanding Molecular Simulation. From Algorithms to Applications*, 2nd ed., Academic Press, San Diego, **2002**.
[32] Y. Sugita, Y. Okamoto, *Chem. Phys. Lett.* **1999**, *314*, 141–151.
[33] R. Yamamoto, W. Kob, *Phys. Rev. E* **2000**, *61*, 5473–5476.
[34] Temperatures of 150.0, 156.0, 162.4, 169.0, 176.0, 183.3, 191.0, 199.0, 207.3, 215.8, 224.6, 233.5, 242.7, 252.1, 261.9, 272.2, 283.0, 294.4, 306.4, 319.2, 332.9, 347.4, and 362.8 K at densities between 0.950 and 1.355 g cm^{-3}, with an increment of 0.015 g cm^{-3}.
[35] S. Nosé, *Mol. Phys.* **1984**, *52*, 255–268.
[36] W. G. Hoover, *Phys. Rev. A* **1985**, *31*, 1695–1697.
[37] S. Miyamoto, P. A. Kollman, *J. Comput. Chem.* **1992**, *13*, 952–962.
[38] U. Essmann, L. Perera, M. L. Berkowitz, T. A. Darden, H. Lee, L. G. Pedersen, *J. Chem. Phys.* **1995**, *103*, 8577–8593.
[39] The *PVT* data are available from http://ganter.chemie.uni-dortmund.de/TIP4PEw.html.
[40] W. Wagner, A. Pruß, *J. Phys. Chem. Ref. Data* **2002**, *31*, 387–535.